Journal of
Marine Science and Engineering

MDPI

Article

Long-Term Contamination of the Arabian Gulf as a Result of Hypothetical Nuclear Power Plant Accidents

Vladimir Maderich *, Roman Bezhenar, Ivan Kovalets, Oleksandr Khalchenkov and Igor Brovchenko

Institute of Mathematical Machine and System Problems, 03187 Kyiv, Ukraine
* Correspondence: vladmad@gmail.com

Abstract: Long-term consequences of radionuclide contamination of the Arabian Gulf as a result of hypothetical accidents at the Bushehr and Barakah nuclear power plants (NPPs) were studied using a chain of models including the atmospheric dispersion model RIMPUFF, the marine compartment model POSEIDON-R, and the dose model. The compartment model POSEIDON-R is complemented by a dynamic model of the biota food chain that includes both pelagic and benthic organisms. The source terms for the hypothetical releases of the selected radionuclides (^{134}Cs, ^{137}Cs, ^{106}Ru, and ^{90}Sr) in the atmosphere were defined as a fraction of respective reactor inventories available in the literature. Conservative meteorological scenarios for the calculation of the initial depositions of radionuclides were selected. Because the Gulf is shallow, a significant portion of the reactive radionuclides (^{134}Cs, ^{137}Cs, ^{106}Ru) remain in the bottom sediments and continue to contaminate water and benthic organisms for a long period of time. The annual dose due to the consumption of marine products can exceed 1 mSv, whereas the annual dose due to drinking the water from desalination plants is expected to be an order less. The contribution of elements to the dose depends on the type of reactor. This is manifested in differences between the contributions of different marine organisms to the dose.

Keywords: Arabian Gulf; radionuclide contamination; Bushehr nuclear power plant; Barakah nuclear power plant; compartment model; nuclear accident

Citation: Maderich, V.; Bezhenar, R.; Kovalets, I.; Khalchenkov, O.; Brovchenko, I. Long-Term Contamination of the Arabian Gulf as a Result of Hypothetical Nuclear Power Plant Accidents. *J. Mar. Sci. Eng.* **2023**, *11*, 331. https://doi.org/10.3390/jmse11020331

Academic Editor: Christos Tsabaris

Received: 25 December 2022
Revised: 21 January 2023
Accepted: 22 January 2023
Published: 3 February 2023

1. Introduction

The Arabian Gulf (hereafter: Gulf) is a shallow body of water connected to the Indian Ocean by the Strait of Hormuz. The average depth of the Gulf is about 30 m. The eastern part of the Gulf is deeper, with depths reaching 60 m. Evaporation in the Gulf exceeds precipitation and river inflow, so that it is an inverted estuary in which saltier and warmer water flows out of the Gulf in a relatively deep trough through the Strait of Hormuz, whereas less saline water spreads into the upper layer along the Gulf. Over the past half-century, the Gulf countries have been experiencing intensive economic development, which has significantly increased energy consumption, particularly for seawater desalination. Over 567 desalination plants were operational in the Gulf in 2018, with a total capacity of 21,180,000 m^3 day^{-1} [1]. The rapid growth in energy consumption in the Gulf States has led to the emergence of nuclear power plants (NPPs) in this region. The first of these was the Bushehr NPP (Iran), which has been operating since 2013. It consists of three VVER-1000 nuclear reactors (one is operating, and two are under construction). The second one is Barakah NPP (UAE). It has been operating since 2021 and consists of four APR-1400 nuclear reactors (three operating, and one undergoing post-construction testing). Several new NPPs are slated for construction by Saudi Arabia in the near future. Globally, the capacity of nuclear power plants is growing steadily, with about 60 reactors under construction [2]. Note that of the 29 reactors to be launched by 2025, 19 are located on the coasts. Therefore, as a result of potential accidents at NPPs, not only land and inland waters, but also ocean waters can be contaminated. Accidental releases of radionuclides from NPPs into the environment can result from natural disasters, technogenic accidents, and military operations. Two examples of accidents of this kind are the largest nuclear accidents that took place at the Fukushima Daiichi NPP [3,4] and the Chernobyl NPP [5]. There is still a danger of damage to the Zaporizhzhia NPP, with the subsequent release of radioactivity into the environment, as a result of the Russian invasion of Ukraine. An example of such a hypothetical accident and its probable impact on the marine environment and people is discussed in [6].

Numerical models are an effective tool to assess the concentration of radionuclides in the marine environment as a result of an accident. Three stages after an accident were defined [7]: the emergency phase (days-weeks), the post-emergency phase (weeks-months), and the long-term phase (months-years). Three main classes of transport models are used to describe the corresponding phases after an accident: Lagrangian, Eulerian, and compartment (box) models. A detailed analysis of the advantages and disadvantages of such models as applied to emergencies is presented in the review detailed in [7]. Recently, Lagrangian models have been used to estimate the emergency and post-emergency phases of radioactive contamination of the coastal waters of the Western Mediterranean, the Eastern Mediterranean, and the Arabian Gulf as a result of a hypothetical accident at a nuclear power plant [8–10]. The Euler model was used to simulate the results of potential accidents at four NPPs located on the shores of the Yellow and East China Seas [11], whereas both Lagrangian and Eulerian models were applied to the hypothetical accident at an NPP located in the Yellow Sea [12]. An accurate specification of the source and a description of atmospheric transport [3–5,13], with the corresponding deposition of radionuclides, predetermines the results of modeling the transport of radionuclides in the sea.

In the relatively shallow Gulf, with limited water exchange through the Strait of Hormuz, the consequences of any accident at an NPP can be long-term, since a significant part of released radionuclides will be deposited in the bottom, which serves as a source of water contamination for an extended period of time. Only a few models of radioactivity transfer to the sea have been applied to the Gulf. To simulate the potential dispersion of radioactivity as a result of the accidental release of radioactivity from the Bushehr NPP into the sea, the CROM model (https://www.researchgate.net/publication/314243628_CROM_8_-_Integrated_dose_assessments_for_humans_and_non-human_biota, accessed on 1 October 2022), based on the Gaussian approach [14], was used in [15,16]. A particle-tracking model to simulate radionuclide transport in the Gulf was developed [9] as a fast response tool after a nuclear accident. This model uses the tidal submodel and the HYCOM model [17] for baroclinic currents forecasts. The Lagrangian algorithms were used for the simulation of the radionuclide transfer in water and sediment. However, the lead time in such predictions is limited by the lead time of meteorological and oceanographic forecasts, which does not currently exceed two weeks.

Nevertheless, there is a need to assess the long-term consequences of potential accidents at NPPs in the Gulf for the marine environment and humans. The compartment models are well suited for these tasks [7]. The aims of our study are (i) to simulate the transport of radionuclides deposited at the Gulf's surface as a result of radioactivity released into the atmosphere caused by hypothetical accidents at two operating NPPs in the Gulf; (ii) to simulate the transfer of radioactivity in the marine food chain; and (iii) to estimate human doses through the marine pathways. A chain of models was used in our study. It includes the atmospheric dispersion model RIMPUFF [18], the marine compartment model POSEIDON-R [19], complemented by the dynamic model of biota food chain, and the dose model, which are integrated into the EU real-time on-line nuclear emergency response system JRODOS [20]. The paper is organized as follows. The atmospheric dispersion model is briefly considered in Section 2.1, the source terms for atmospheric release are considered in Section 2.2, and the compartment model is described in Section 2.3. The setup of the models, the forcing, and the scenarios of the accidents are given in Section 2.4. The results of the calculations of the radionuclide concentrations in the water, sediment, and biota for the scenarios of potential release from the Bushehr and Barakah NPPs are discussed in

Sections 3.1 and 3.2. The doses for humans are estimated in Section 3.3. Our findings are discussed in Section 4.

2. Materials and Methods

2.1. Atmospheric Dispersion Model RIMPUFF

The algorithm of the atmospheric dispersion model (ADM) RIMPUFF replaces a continuous release with a series of consecutively released puffs. At each time step, the model equations describe the advection, diffusion, and deposition of the individual puffs, according to local meteorological conditions. A modified RIMPUFF model [18] combines computational efficiency with advanced algorithms for the assessment of the puff's growth at medium-range time and spatial intervals of atmospheric transport. The dry deposition on the water surface in JRODOS RIMPUFF is calculated using the value of the dry deposition velocity $v_d = 0.0007$ m s^{-1}. In the calculation of the wet deposition, the value of wash-out coefficient χ [s^{-1}] is calculated using the usual formula: $\chi = \Lambda\left(I/I_{ref}\right)^{\alpha}$, where I [mm h^{-1}] is the precipitation rate, $I_{ref} = 1$ mm h^{-1} is the reference precipitation rate, and the values of the parameters are $\Lambda = 8 \cdot 10^{-5}$ s^{-1}; $\alpha = 0.8$. A more detailed technical description of RIMPUFF is available on the JRODOS site [20]. The RIMPUFF model has been extensively validated against measurement data collected in numerous field experiments and full-scale accidents, including Fukushima [21]. For ensuring the robustness of the obtained results in this study, we also performed sensitivity tests of the calculated deposition with the Lagrangian ADM DIPCOT [22], which is also included in the atmospheric dispersion module of the JRODOS system, using the same parameterizations of dry and wet deposition.

2.2. Source Terms for Atmospheric Releases from Bushehr and Barakah NPPs

The source terms for the hypothetical releases of the radionuclides in the atmosphere considered in this study from the Bushehr and Barakah NPPs were defined based on respective reactor inventories available in the literature. For the Bushehr NPP which operates the VVER-1000 reactor, the inventory was taken from the study in [23]. The released fractions of the inventory corresponded to the most conservative assessments of the Ukrainian National Atomic Generating Company NAEK "Energoatom," performed for the VVER-1000 reactor of the Zaporizhzhia NPP for the scenario of the "full loss of electric power supply together with loss of coolant with taking into account actions on reducing hydrogen concentration" [24]. For the Barakah NPP, which operates the APR-1400 reactor, the inventory was taken from the figures in reference [25]. The same emitted fractions of the inventory for the Barakah NPP were assumed as those for Bushehr NPP. Only the long-lived radionuclides (half-life $T_{1/2} > 1$ year), which were of interest for long-term assessment of water contamination, and doses from aquatic pathways were considered in this study. Based on the analysis of the above data, the following radionuclides were selected for simulation: ^{134}Cs, ^{137}Cs, ^{106}Ru, and ^{90}Sr. The corresponding released fractions of inventories, together with the released inventories in Bq from the Bushehr and Barakah NPPs of the four considered radionuclides for these hypothetical accidents, are presented in Table 1. According to reference [24], the total period of release (25 h) was split into two parts. The largest quantities of strontium and cesium were emitted during the first 3 h of the release (Table 1), while the largest quantity of ruthenium (97%) was emitted later due to the high melting temperature of this radionuclide. The estimates of the released inventories of other long-lived radionuclides, such as ^{239}Pu and ^{244}Cm, according to the described approach, were at least by 3 orders of magnitude smaller than the inventories of the selected radionuclides presented in this paper. Therefore, they were not considered in this study.

Table 1. Released fractions of inventories and corresponding activities of radionuclides for hypothetical accidents at the Bushehr and Barakah NPPs.

Radionuclide	Released Fraction of Inventory, %	Released Inventory, Bq (Bushehr NPP)	Released Inventory, Bq (Barakah NPP)	% of Emission during First 3 h
^{134}Cs	3.4	4.93×10^{16}	4.69×10^{16}	91
^{137}Cs	3.4	9.86×10^{15}	2.60×10^{16}	91
^{106}Ru	≤ 17.7	5.07×10^{16}	9.35×10^{17}	3
^{90}Sr	1.3	3.46×10^{15}	6.67×10^{15}	80

2.3. Marine Compartment Model POSEIDON-R

The basic feature of marine compartment models (the uniform distribution of radionuclides within each compartment) decreases the calculation time and makes these models useful tools in the long-term phase of an emergency after an accident [7]. In the POSEIDON-R model [26–28], the marine environment is represented as a system of compartments for the water column, bottom sediment, and biota. The compartment-averaged radionuclide concentration is governed by a set of ordinary differential equations describing the temporal variations of the concentration, the exchange with adjacent compartments, and with the suspended and bottom sediment, radioactive sources, and decay. The exchange between the water column boxes is described by fluxes in the radionuclides due to advection, sediment settling, and turbulent diffusion processes (Figure 1). The additional diffusion fluxes of water between boxes were included to take into account mixing by tides [27]. The model equations were complemented by the term describing the flux of the radionuclides from the upper sediment layer to the water due to resuspension processes, which are important in the case of intensive tidal currents. A detailed description of the model and the numerical algorithm is given in [27].

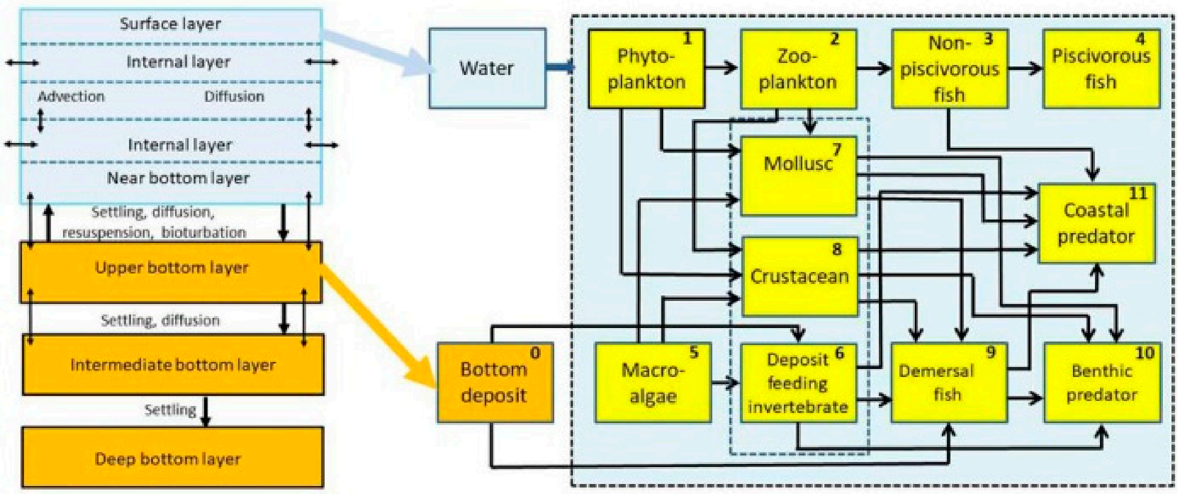

Figure 1. Structure of a compartmental system in the POSEIDON-R model, including radionuclide transfers from the water and bottom sediment boxes to marine organisms. The radionuclide transfers among marine food web compartments are given for 11 types of marine organisms. The large blue rectangle shows the uptake activity of every organism from water. Arrows show the pathways of the radionuclides between the boxes and organisms in the food chain.

Unlike other marine compartment models, POSEIDON-R uses the dynamic food chain model, which is necessary for the modeling of the consequences of accidental releases [11]. This model was extended by the inclusion of benthic organisms [28], which is especially important for a shallow Gulf. A scheme of the radionuclide transfer through the marine food chain is shown in Figure 1. The model includes pelagic and benthic food chains. Pelagic organisms are grouped into phytoplankton, zooplankton, non-piscivorous, and piscivorous fishes. Benthic organisms include deposit-feeding invertebrates, demersal fish, and bottom predators. Coastal predators feed on both pelagic and benthic organisms in shallow waters. Detritus feeders and filter feeders are presented by crustaceans and mollusks, respectively.

For the simulation of the uptake and retention of radionuclides in marine organisms, which form the food web, the whole-body dynamical model is used. An exception is phytoplankton, where the concentration of radioactivity is calculated using the biological concentration factor (BCF) [29] which refers to uptake from the water. In the model, the concentration of radionuclide in the whole body (wb) of each considered organism C_{wb} is described by the equation

$$\frac{dC_{wb}}{dt} = AE_w K_w C_w + AE_f K_f C_f - \lambda_{wb} C_{wb}, \tag{1}$$

where AE_w and AE_f are assimilation efficiencies for the uptake of radionuclides from water and food, K_f and K_w are food and water uptake rates, C_w and C_f are concentrations of radionuclide in water and food, and λ_{wb} is the elimination rate of radionuclide from the organism. Eleven types of organisms were considered in the model (Figure 1), which form pelagic and benthic food chains. The concentration of radioactivity in food for a predator C_f is calculated as a weighted concentration in the prey organisms

$$C_f = \sum_{j=0}^{m} C_{prey,j} P_j \frac{drw_{pred}}{drw_{prey,j}} \tag{2}$$

where $C_{prey,j}$ is the activity concentration in prey of type j, P_j is the preference for prey j, drw_{pred} and $drw_{prey,j}$ are the dry weight fraction of predator and prey of type j, respectively, and m is the number of prey organisms in the diet of the predator. The model parameters for all organisms, except different types of fish, are given in the basic paper for POSEIDON-R [27].

For fish (organisms Nos. 3, 4, 9, 10, and 11 in Figure 1), the tissue-weighted whole-body elimination rate [30] was used as

$$\lambda_{wb} = \sum_{i=1}^{3} \mu_i \lambda_i / R_i \tag{3}$$

where i is the tissue number (i = 1; 2; 3 for bone, muscle, and organ, respectively), μ_i is a mass fraction of the given tissue, λ_i is an elimination rate of activity from i-th tissue, $R_i = C_{wb}/C_i$ and is a whole-body to tissue concentration ratio described in [31]. Such an approach was validated in [30] on the ^{90}Sr release to the marine environment as a result of the Fukushima Daiichi accident, where it gives results similar to the fish multi-compartment MCKA model [30]. The parameters of Equation (1) for fish are given in Table 2. The assimilation efficiencies for the uptake of radionuclides from water and food were estimated from laboratory experiments [32] or were based on the biological accumulation factor (BAF) for fish [29], which also includes uptake from food.

Table 2. Model parameters for the uptake of radioactivity by fish.

Parameter	^{134}Cs, ^{137}Cs	^{90}Sr	^{106}Ru
AE_w	1×10^{-3}	3×10^{-5}	8×10^{-6}
AE_f	0.76 [1]	0.29 [2]	0.006 [2]
λ_{wb}, day^{-1} (prey types Nos. 3, 9)	0.0092	0.0054	0.0164
λ_{wb}, day^{-1} (predatory types Nos. 4, 10, 11)	0.0046	0.0027	0.0082

[1] [32], [2] [29].

The generic parameters of the compartment model POSEIDON-R, with the dynamical food chain model, were validated by the measurement data in different seas and oceans [27,28,30]. The sensitivity analysis was carried out in references [28,30] to estimate parameter sensitivity. A detailed comparison of simulation by POSEIDON-R with other compartment models and Eulerian models of radioactivity transport in the relatively shallow Baltic Sea [33] demonstrated the reliability and robustness of the model for a problem similar to the one considered in this paper.

2.4. Poseidon-R Model Setup

The compartment system for the Arabian Gulf and Gulf of Oman consists of 136 boxes (Figure 2a), including boxes inside and outside the Gulf. In particular, outside boxes (box No.1 represented the World Ocean, and box No. 2 represented the Arabian Sea; they are not shown in the figure) were introduced for the connection of the Gulf with the Ocean. The volume and average depth for each box were calculated using the bathymetry data from [34]. One-layer shallow boxes (depth less than 30 m) are marked in white, whereas deeper two-layer boxes are marked in blue. Water fluxes between boxes were calculated by averaging over 10 years of three-dimensional currents calculated from reanalysis [34]. The time-averaged currents in the surface boxes are shown in Figure 2b.

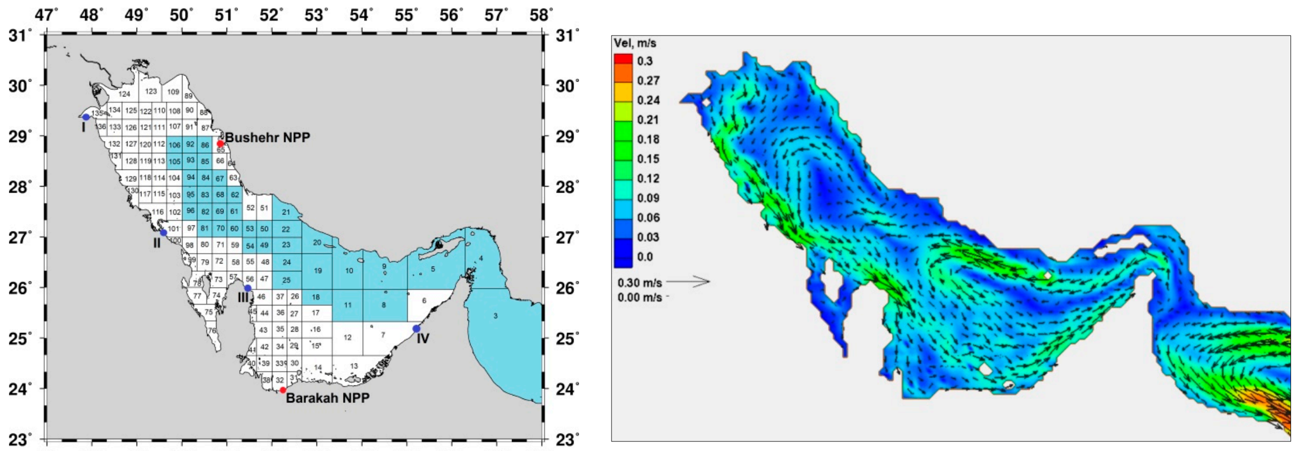

(a) (b)

Figure 2. (**a**) Compartment system for the Arabian Gulf. Deep boxes with two vertical layers in the water column are marked in blue, and shallow one-layer boxes are shown in white. The red-filled circles show operating NPPs. The blue-filled circles show the locations of four desalination plants: I–IV are the Doha, Al Jubail, Ras Laffan, and Jabel Ali plants, respectively. (**b**) Time-average surface currents calculated from ocean reanalysis data [34] in the Arabian Gulf.

The influx of water from the ocean through the Strait of Hormuz and the influx of fresh water through the Shatt al-Arab River (46 km^3 a^{-1} [35]) and other rivers is balanced by evaporation from the Gulf. The fluxes of water between boxes in the surface layer reproduce the time-averaged surface circulation in the Gulf, which is shown in Figure 2b. However, in the subsurface layer that exists in the deep boxes, marked by blue in Figure 2a, the circulation is different. In the Strait of Hormuz, the flux of water in the surface layer is directed into the Gulf, while the flux of water in the subsurface layer is directed out of the Gulf. Similarly, fluxes in the deep boxes in the Gulf differ from fluxes in the surface layer boxes, in agreement with the 3D modeling results [34,35]. Diffusion fluxes were estimated by averaging the fluxes between boxes. We concluded that two-layer parameterization allowed us to correctly represent the structure both of the advection and diffusion processes in the Gulf. Suspended sediment concentration in the water column was set up according to the methods of [36]. Specific sedimentation rates for different parts of the Gulf were adopted from [37]. Default values for other parameters, which are needed for simulations of water-sediment interaction processes, were used in the model [27].

2.5. Scenarios of Atmospheric Deposition

Conservative meteorological scenarios for the calculation of initial depositions of radionuclides on the surface of the Gulf following hypothetical release from the Bushehr and Barakah NPPs were selected as described below. For each of the NPPs, a set of different scenarios of atmospheric dispersion and deposition, using the same source term, but with different start days of release, were calculated with the statistic output tool of the European system of nuclear emergency response JRODOS [20]. This tool randomly generates initial start dates of release within the prolonged time for which meteorological data are available. The average time interval between the generated start dates is 1 day. The calculation of the atmospheric transport model RIMPUFF is then automatically performed for each of the start dates. The simulation time of automatically generated RIMPUFF runs in this study was the same, and was equal to 96 h. The depositions were calculated in the nodes of the largest JRODOS computational grids of the sizes 1600 $\times$ 1600 km, centered at the Bushehr and Barakah NPPs, respectively.

The meteorological data were calculated with the WRF mesoscale meteorological model [38] for the 5 years from 1 January 2014 to 31 December 2018. The computational domain of the WRF covered the computational domains of JRODOS; it had a horizontal resolution of 0.15 deg, and the number of nodes in the South-North and West-East directions was 150 $\times$ 150. The final analysis data of the Global Forecast System (GFS) operated by the US National Centers for Environmental Prediction [39] were used for setting initial and boundary conditions in WRF simulations.

For the Bushehr NPP, the maximum deposition of the radionuclides was obtained for the dispersion scenario, with the start date of the release as 24 December 2015, 08:00 UTC. The total deposited amounts on the sea surface of ^{134}Cs, ^{137}Cs, ^{106}Ru, and ^{90}Sr in this dispersion scenario were: 4.62×10^{16}, 9.25×10^{15}, 3.37×10^{16}, and 3.13×10^{15} Bq, respectively. The deposited amounts constituted 93.8, 93.8, 66.4, and 90.5% of the total released inventories of the ^{134}Cs, ^{137}Cs, ^{106}Ru, and ^{90}Sr, respectively (Table 1). For the Barakah NPP, the maximum deposition of the radionuclides was obtained for the dispersion scenario with the start date of the release as 21 November 2017, 15:43 UTC. In this scenario, the deposition of ^{106}Ru (7.30×10^{17} Bq) was an order of magnitude greater than in the scenario for Bushehr, while the deposited amounts of ^{134}Cs, ^{137}Cs, and ^{90}Sr were of the same order (4.36×10^{16}, 2.43×10^{16}, and 6.10×10^{15} Bq, respectively). The deposited amounts constituted 93.4, 93.4, 78.1, and 91.5% of the total released inventories of the ^{134}Cs, ^{137}Cs, ^{106}Ru, and ^{90}Sr, respectively (Table 1). The described two dispersion scenarios with the maximum deposition on the sea surface were subsequently treated as conservative.

In both accident scenarios, more than 90% of the radionuclides were deposited on the sea surface by the wet removal process. Therefore, the precipitation fields calculated by the WRF model were checked against measurements performed during the selected time intervals by nine meteorological stations located close to the sea border in Iran, Saudi Arabia, and Qatar (Supplementary Table S1). In total, 166 measurements of precipitation and intensities were extracted from the Wolfram database [40] for the periods considered in this study: 24–29 December 2015, and 21–16 November 2017. The correlation coefficient (CC) of the calculated precipitation intensities as compared to the measurements was CC = 0.39, with a mean absolute error (MAE) = 12.9 mm day^{-1}. The results for the correlation coefficient and MAE are in agreement with the estimated accuracy of the satellite-derived precipitation fields evaluated for several rainfall events in Saudi Arabia in [41]: $0.008 \leq$ CC ≤ 0.58, $3.6 \leq$ MAE ≤ 17.8 mm day^{-1}. The relative bias of the precipitation calculated by WRF in this study as compared to the measurements was RB = -45%, Therefore the amount of wet deposition was not overestimated in the considered scenarios. The comparisons of precipitation intensities calculated by WRF, with respective measurements, are presented in Supplementary Figures S1 and S2.

The reported total amount deposited on the surface of the Gulf did not change significantly when ADM DIPCOT was applied for the same meteorological scenario (Table S2 in Supplementary Materials). In both simulated cases and for the radionuclides ^{134}Cs, ^{137}Cs, and ^{90}Sr, the differences in the respective deposited amounts were within 5% of the above presented values. The differences in the deposited amount of ^{106}Ru between RIMPUFF and DIPCOT were within 16%—somewhat higher than for other radionuclides due to a more uniform time distribution of the release of ^{106}Ru as compared to other aerosols. Such differences are still not significant, taking into account considerable differences in the modeling approaches of both ADMs. The deposition maps ^{137}Cs, ^{134}Cs, ^{106}Ru, and ^{90}Sr from the conservative dispersion scenarios for the Bushehr (Figures 3a and S3) and Barakah (Figures 3b and S4) NPPs were further used for the assessment of radionuclide concentrations in the water and sea products.

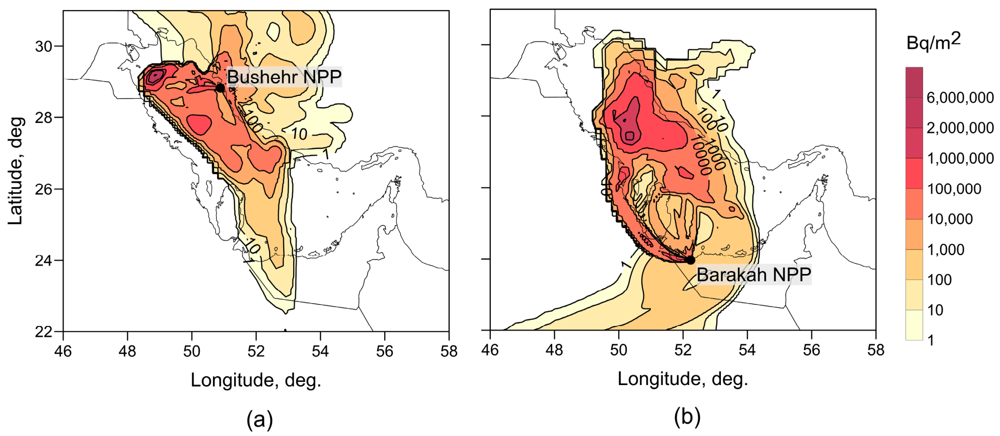

Figure 3. (**a**) Map of total (dry + wet) deposition density of ^{137}Cs simulated by the JRODOS system for the hypothetical accident scenario at the Bushehr NPP started on 24 December 2015, 08:00 h UTC; (**b**) map of total (dry + wet) deposition density of ^{137}Cs simulated by the JRODOS system for the hypothetical accident scenario at the Barakah NPP started on 21 November 2017, 15:43 h UTC; deposition maps are dated 96 h after the start of the respective accident scenario.

3. Results

3.1. Bushehr NPP

The maximum simulated distribution of ^{137}Cs deposition was in the northwestern part of the Gulf off the coast of Kuwait (Figure 3a). The distribution of ^{134}Cs and ^{90}Sr was basically like the distribution of ^{137}Cs, while the distribution of ^{106}Ru was different due to the delay of release (Figure S3). The spatial distribution of the ^{137}Cs concentration in the surface waters of the Gulf after deposition for the hypothetical accident scenario at the Bushehr NPP is shown in Figure 4. The corresponding distributions of ^{134}Cs, ^{90}Sr, and ^{106}Ru are given in Supplementary Figures S5–S7. Since the maximum deposition of radionuclides under the selected meteorological conditions was in the north-western part of the Gulf, the maximum concentrations of the radionuclides in the water initially occurred there. Over time, the contamination is transported by currents (see Figure 2b) along the coast of the Arabian Peninsula to the Strait of Hormuz. Corresponding temporal changes in the surface concentration of the radionuclides in the locations of four desalination plants (see Figure 2a) due to the hypothetical accident scenario at the Bushehr NPP are given in Figure 5. As follows from the graphs, the maximum concentrations of radionuclides and the intervals between the deposition time and these maximums depend on the position of the desalination plants and the properties of the radioisotopes. The maximum concentration of radionuclides at the Doha plant is reached after 5–6 months, at the Al Jubail plant after 10 months, and at the Ras Laffan plant after 14 months, while at the Jabel Ali plant, it is reached after 2.5–3 years, except for ruthenium, for which the maximums are reached within the first year. However, maximal concentrations at each desalination plant are significantly different and decrease with the distance from the deposition maximum.

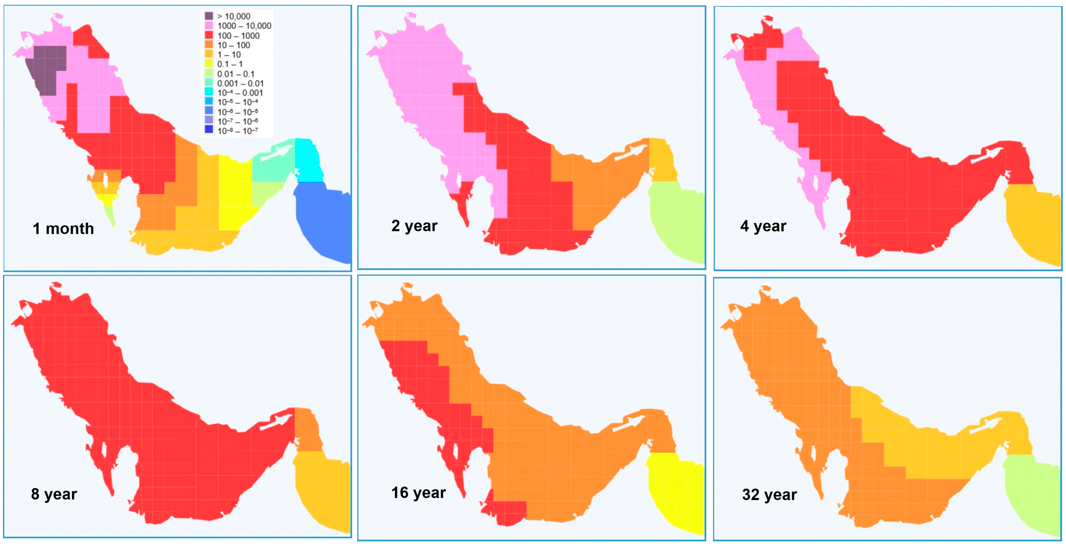

Figure 4. Temporal change in the distribution of the ^{137}Cs concentration in water (Bq m^{-3}) at the Arabian Gulf surface after deposition for the hypothetical accident scenario at the Bushehr NPP.

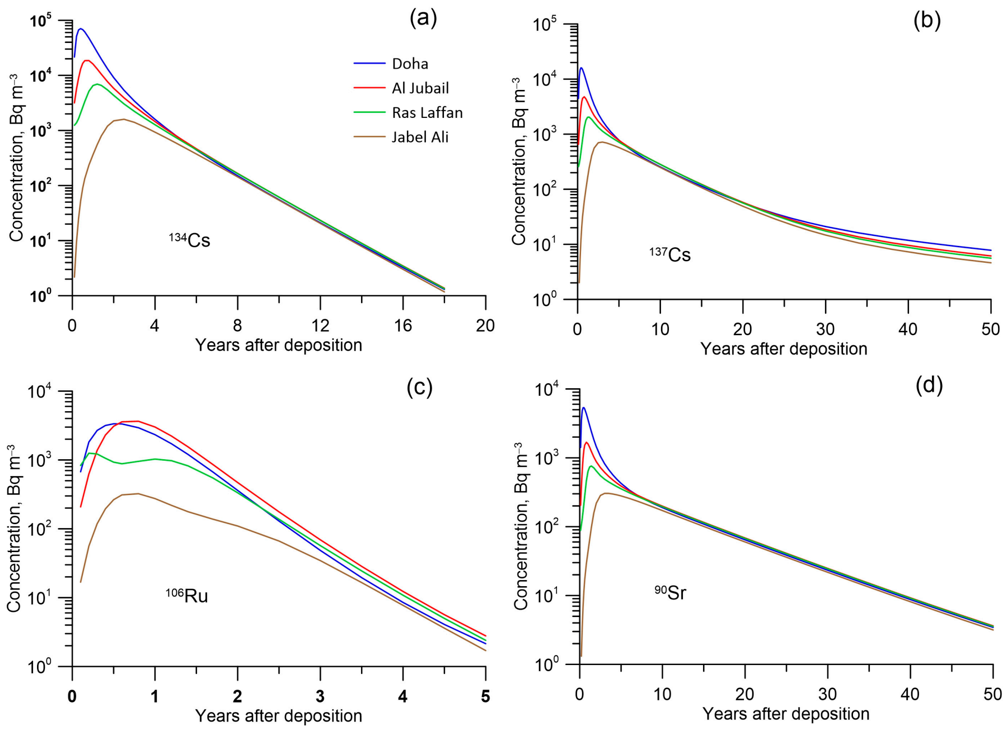

Figure 5. Temporal change in surface concentration (Bq m^{-3}) of ^{134}Cs (**a**), ^{137}Cs (**b**), ^{106}Ru (**c**), and ^{90}Sr (**d**) in locations of selected desalination plants (see Figure 2a) due to the hypothetical accident scenario at the Bushehr NPP.

In the shallow Gulf, the distribution pattern of bottom contamination is mainly determined by the distribution of radionuclides deposited on the sea from the atmosphere (Figure 6 and Supplementary Figures S8–S10). At the same time, the process of the transfer of nuclides from the water column to the bottom sediments continues for a long time, increasing the bottom contamination despite the decay of radioactivity, redissolution, and resuspension of sediments. This is confirmed by the plots of temporal change of inventory in the water and bottom sediments, seen in Figure 7. The maximum inventories of long-lived isotopes ^{137}Cs ($T_{1/2}$ = 30 y), and ^{90}Sr ($T_{1/2}$ = 28.8 y) in the bottom sediments are reached in the 10th and 7th years, respectively. For ^{134}Cs ($T_{1/2}$ = 2.1 y) and ^{106}Ru ($T_{1/2}$ =

373 d), these maximums are reached at 2.5 years and 1 year, respectively. Except for ^{90}Sr, the sediment inventory will exceed the water inventory starting from the 7th year for ^{134}Cs and ^{137}Cs and from 10th month, for ^{106}Ru. The predominance of the inventory of reactive elements released in the sea in the bottom sediments as a result of the accident is typical for shallow seas. After sufficiently long periods (tens of years), the water and sediment inventory decay exponentially due to radioactive decay and dilution through the Strait of Hormuz. At the same time, the concentration of ruthenium in the water and bottom sediments is close to equilibrium.

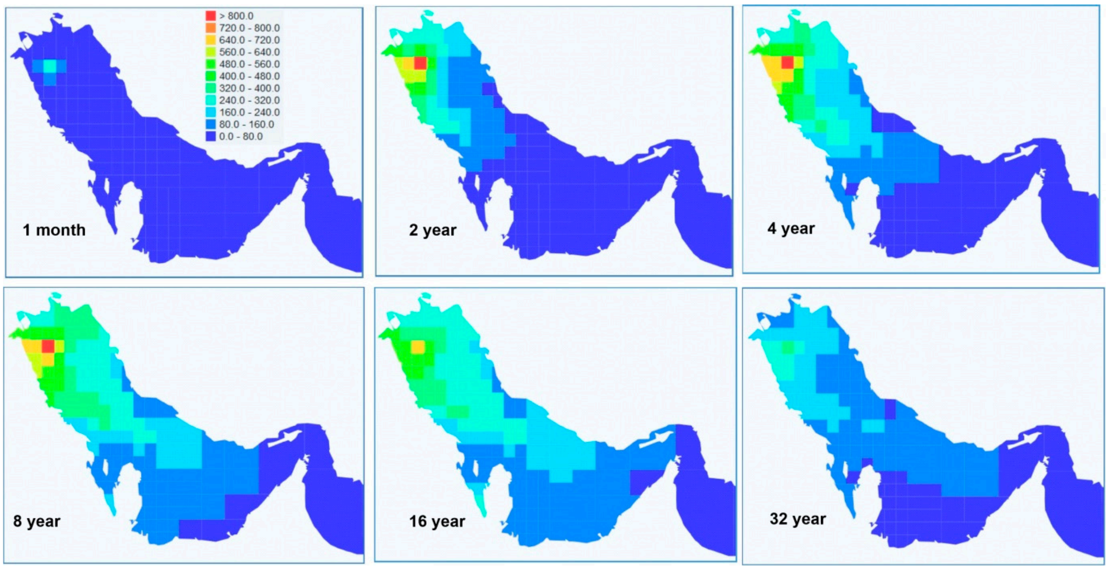

Figure 6. Temporal change in the distribution of ^{137}Cs concentration in the Arabian Gulf upper bottom sediment layer (Bq kg^{-1}) after deposition due to the hypothetical accident scenario at the Bushehr NPP.

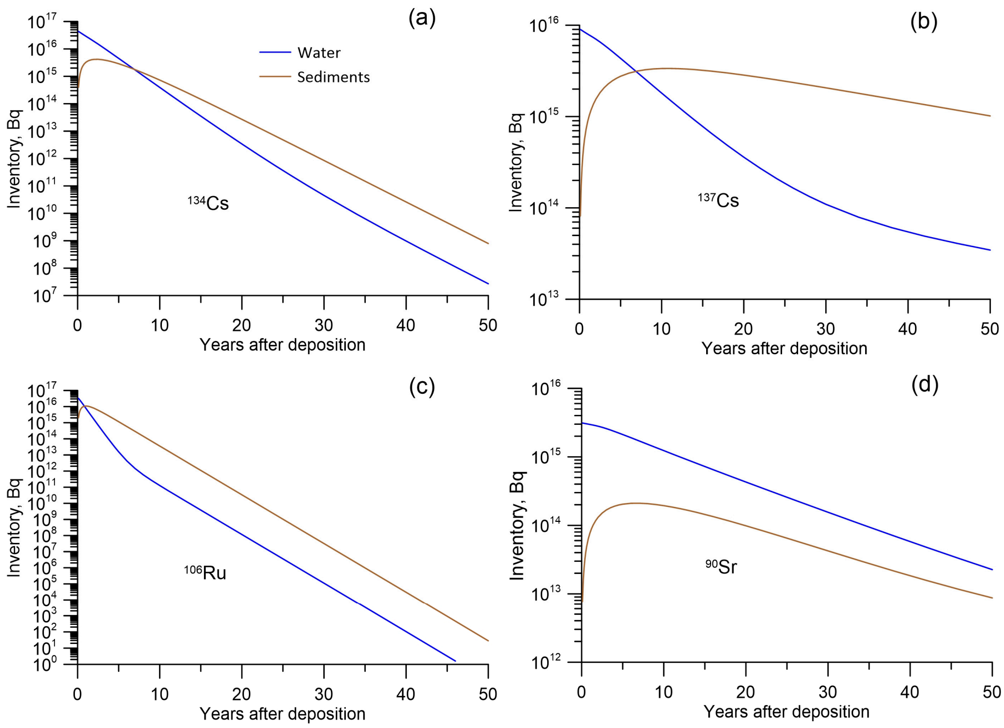

Figure 7. Temporal change in inventory (Bq) of ^{134}Cs (**a**), ^{137}Cs (**b**), ^{106}Ru (**c**), and ^{90}Sr (**d**) in the Arabian Gulf as the result of the hypothetical accident scenario at the Bushehr NPP.

The highest concentration of radionuclides in fish was obtained in box 126 near the Saudi Arabian coast. As can be seen from Figure 8, in the initial period after the accident (first year) the highest concentration of all radionuclides is expected in pelagic non-piscivorous fish. Later concentrations in other types of fish could be higher than in non-piscivorous fish, but do not exceed its initial maximum. For both isotopes of cesium, the concentrations in predatory types of fish will exceed the concentrations in non-piscivorous fish because cesium can accumulate in the food chain (from lower to higher trophic levels). Ruthenium has no such ability, and its concentration decreases in the food chain. Ruthenium accumulates in these types of fish that consume mollusks and crustaceans in their diets because mollusks and crustaceans accumulate ruthenium more efficiently, which is confirmed by the BAF values [29]. Moreover, strontium does not accumulate in the food chain. After some time, when the concentration of radionuclides in water decreases due to the influx of clean water from the Indian Ocean, bottom sediments become the most contaminated component of the Gulf, as seen in Figure 7a–c and Supplementary Figures S8 and S9. Therefore, the demersal fish become the most contaminated type of fish. This is valid for all radionuclides considered, except for ^{90}Sr, which is characterized by a low K_d value, which corresponds to the lower deposition of this nuclide in bottom sediments (Figure 7d and Figure S10).

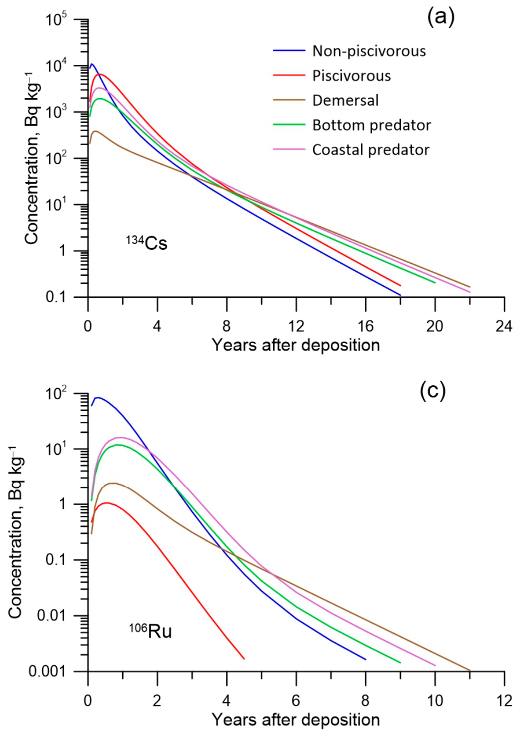

Figure 8. Temporal change of the concentration in different types of fish (Bq kg^{-1} wet weight) of ^{134}Cs (**a**), ^{137}Cs (**b**), ^{106}Ru (**c**), and ^{90}Sr (**d**) in box No. 126 as a result of the hypothetical accident scenario at Bushehr NPP.

Because the Gulf is shallow, most of the reactive radionuclides (^{134}Cs, ^{137}Cs, ^{106}Ru) remain in bottom sediments and continue to contaminate water and benthic organisms for a long time. Even 50 years after the hypothetical accident, the concentration of ^{137}Cs in bottom sediments will be about 30 times higher than the current background concentration, which is 1–3 Bq kg^{-1} [42]. The corresponding simulated concentration of ^{137}Cs in water was 5–8 Bq m^{-3}, whereas the current background concentration was 1.25–1.38 Bq m^{-3} [42]. Therefore, 50 years after radioactive release, the concentration of ^{137}Cs in fish varies between 0.5 Bq kg^{-1} wet weight (WW) for non-predatory fish and 6.7 Bq kg^{-1} WW for the coastal predators, whereas the current background concentration in predatory fish is less than

0.034 Bq kg^{-1} WW [42]. Such a distribution of reactive radionuclides between water and sediments when the inventory in the bottom sediments is dominant over a long time period is typical for shallow seas and shelves [11].

3.2. Barakah NPP

The distribution of deposition from the Barakah NPP on the surface of the Gulf, as well as for the hypothetical accident at the Bushehr NPP, was chosen to be maximal. Therefore, the Barakah deposition area was also extended along the Gulf. However, the corresponding maximum level of deposition was closer to Qatar, as seen in Figure 3b. The distributions of ^{134}Cs and ^{90}Sr were also similar to the distribution of ^{137}Cs, while the distribution of ^{106}Ru was slightly different (Figure S4). The spatial distribution of the ^{137}Cs concentration in surface waters of the Gulf after deposition resulting from the hypothetical accident scenario at Barakah NPP is shown in Figure 9. The corresponding distributions of ^{134}Cs, ^{90}Sr, and ^{106}Ru are given in Supplementary Figures S11–S13. Over time, the ^{137}Cs contamination is dispersed by currents in the Gulf. The coastal area of the Arabian Peninsula after 8 years remains more contaminated than the coast of Iran (see Figure 9).

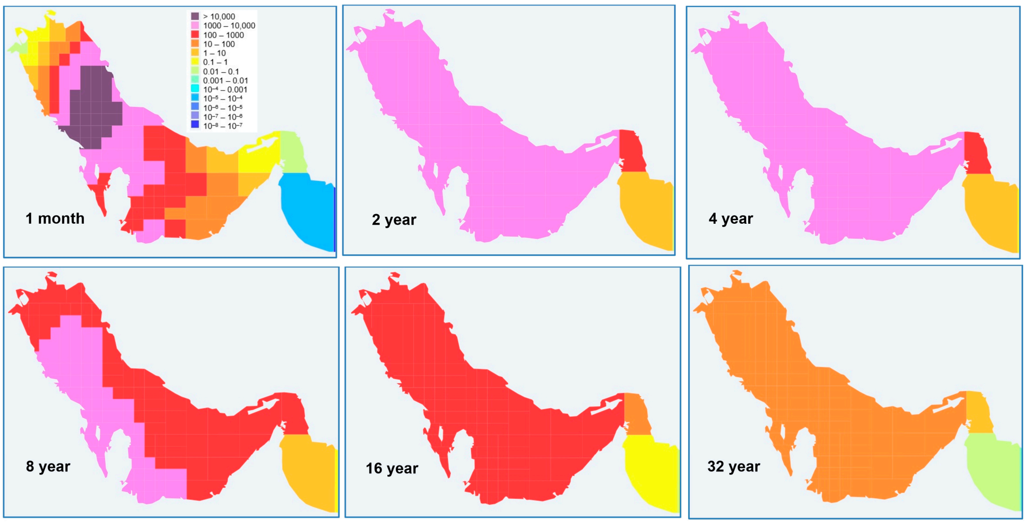

Figure 9. Temporal change in the distribution of the ^{137}Cs concentration in water (Bq m^{-3}) at the Arabian Gulf surface after deposition due to the hypothetical accident scenario at the Barakah NPP.

The temporal changes in the surface concentration of the radionuclides in the locations of four desalination plants (see Figure 2a) due to the hypothetical accident scenario at the Barakah NPP are given in Figure 10. The maximum concentrations of radionuclides and the intervals between the deposition time and these maximums at the desalination plant locations differ from the Bushehr NPP scenario due to the release scenario. The maximum concentration of radionuclides at the Doha plant is reached after 2 years, at the Al Jubail plant after 2 months, and at the Ras Laffan plant after 6 months, while at the Jabel Ali plant, it is reached after 2 years, except in the case of ruthenium, where the maximums are reached within the first year.

Similar to the Bushehr NPP scenario, the distribution pattern of bottom contamination is mainly determined by the distribution of radionuclides deposited onto the sea from the atmosphere (Figure 11 and Supplementary Figures S14–S16). The process of the transfer of reactive long-lived radionuclides from the water column to the bottom sediments continues for a long period of time. Therefore, the maximums of the inventories of the long-lived isotopes ^{137}Cs and ^{90}Sr were reached 10 and 11 years after release, respectively (Figure 12). A total of 50 years after the release of ^{137}Cs, its inventory in the bottom sediments exceeds the inventory in the water by 30 times.

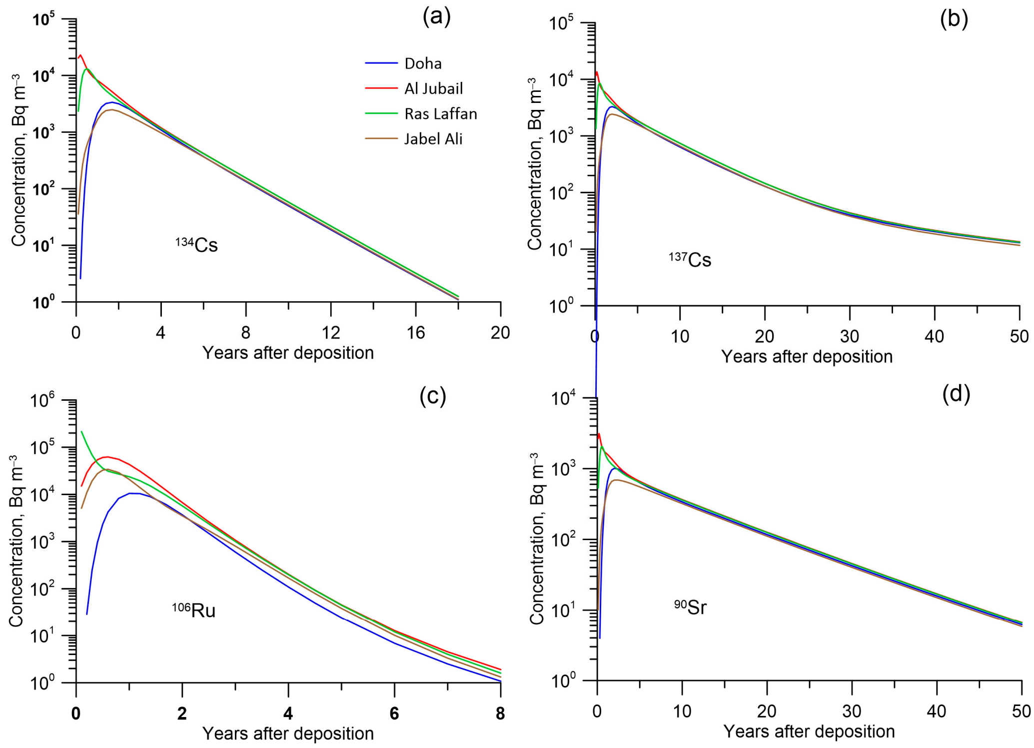

Figure 10. Temporal change in the surface concentration (Bq m^{-3}) of ^{134}Cs (**a**), ^{137}Cs (**b**), ^{106}Ru (**c**), and ^{90}Sr (**d**) in locations of selected desalination plants (see Figure 2a) as the result of the hypothetical accident scenario at the Barakah NPP.

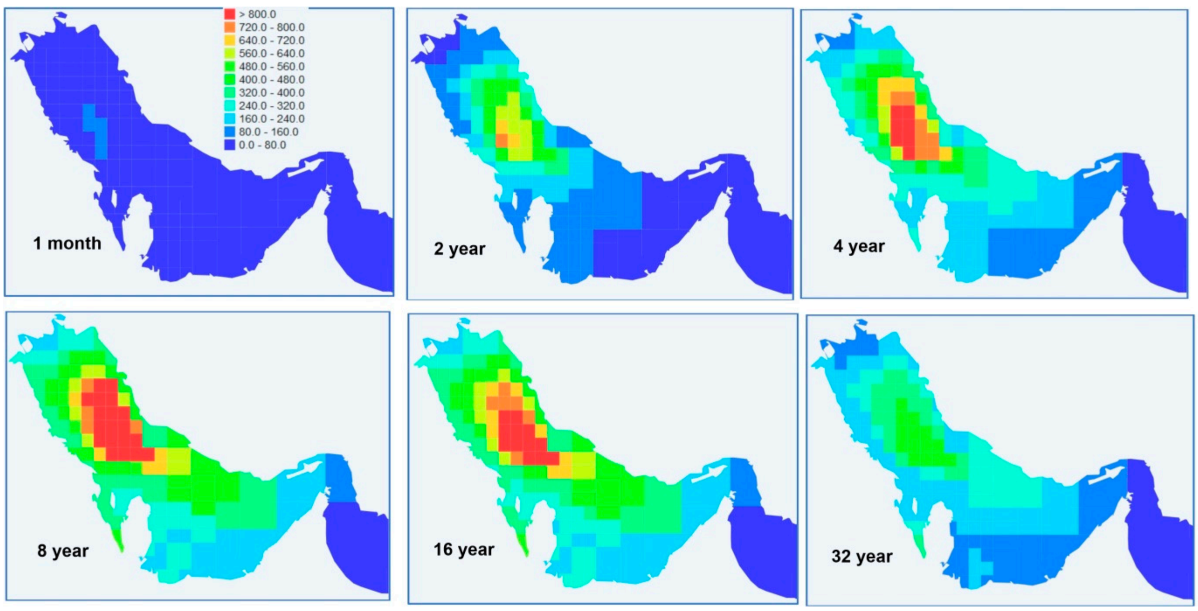

Figure 11. Temporal change in the distribution of ^{137}Cs concentration in the Arabian Gulf upper bottom layer (Bq kg^{-1}) after deposition due to the hypothetical accident scenario at the Barakah NPP.

The highest simulated concentration of radionuclides in fish for the Barakah NPP scenario was in box 95. The distribution of radionuclides between fish species (Figure 13) is generally similar to the distribution in the scenario for the Bushehr NPP, except in the case of ^{106}Ru, whose concentration in fish is an order of magnitude higher, in accordance with the deposition scenario (see discussion in Section 4).

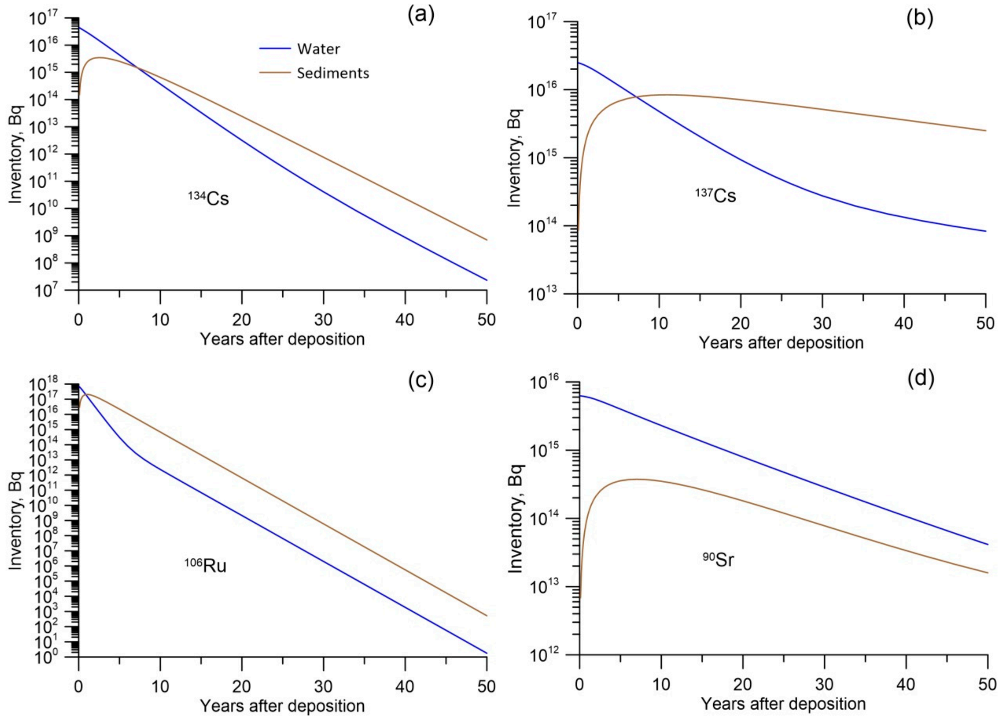

Figure 12. Temporal change in the inventory (Bq) of ^{134}Cs (**a**), ^{137}Cs (**b**), ^{106}Ru (**c**), and ^{90}Sr (**d**) in the Arabian Gulf as a result of the hypothetical accident scenario at the Barakah NPP.

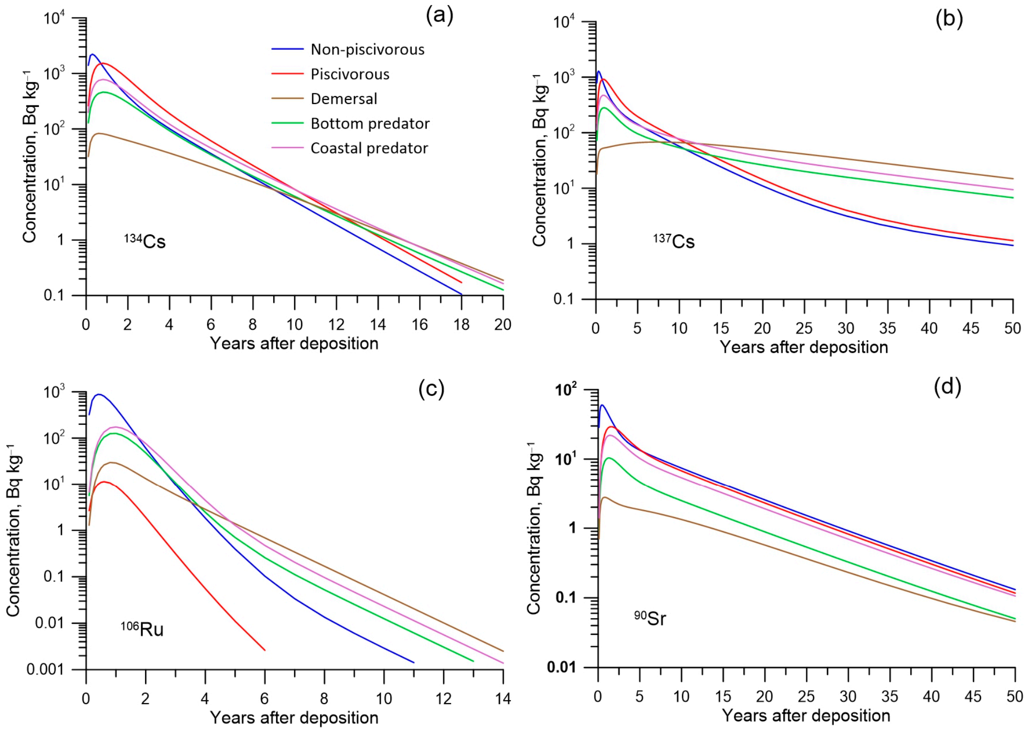

Figure 13. Temporal change in the concentration (Bq kg^{-1} wet weight) of ^{134}Cs (**a**), ^{137}Cs (**b**), ^{106}Ru (**c**), and ^{90}Sr (**d**) in box No. 95 as a result of the hypothetical accident scenario at the Barakah NPP.

3.3. Doses for Humans

In general, there are marine, terrestrial, and atmospheric pathways of human exposure resulting from the release of radioactive materials in the environment. Doses from the contamination cloud (external exposure) and the inhalation of contaminated air (internal exposure) are related to the atmospheric pathway. Atmospheric deposition on the land contaminates the ground (external exposure), and deposited radionuclides circulate in the terrestrial food web, which is the basis of human nutrition (internal exposure). Marine pathways also include internal exposure, i.e., doses from the ingestion of seafood, drinking of desalinated water (if applicable), inhalation of sea spray; and external exposure, i.e., doses from swimming, boating, and shoreline activity. All these pathways have to be assessed in the case of a real accident. The current study is focused on marine pathways of human exposure, while other dose pathways will be considered in future studies.

The effective annual dose ($Sv \cdot a^{-1}$) for humans from marine product consumption was calculated based on those obtained for the model concentrations of radionuclides in marine organisms using the formula:

$$E_{ing,k} = DC_k \sum_{p=1}^{6} C_{p,k} CR_p \tag{4}$$

where $E_{ing,k}$ is the annual dose (Sv a^{-1}) of k-th radionuclide from the consumption of marine products from six categories (p) of marine organisms (crustaceans (shrimp) and five types of fish), DC_k is the dose coefficient for k-th radionuclide due to the ingestion of contaminated food for adults [43,44], $C_{p,i}$ is the calculated concentration of activity of k-th radionuclide in the marine product of type p, and CR_p is the annual human intake rate (kg a^{-1}) of the marine product of type p. To obtain a conservative estimation of the dose, the box with a maximal concentration of radionuclides in marine products was chosen for dose calculation.

To define the annual consumption rate of marine products, the FAO data [45] regarding fishery production and consumption in Kuwait, Saudi Arabia, Qatar, Iran, and UAE were analyzed. As a conservative assumption, the averaged data for reference persons in the region were used for dose calculation. The reference person was considered as a person who consumes marine products only from the Gulf. The average of the six considered countries' annual consumption rates of 15.2 kg a^{-1} for fish and 2.07 kg a^{-1} for crustaceans were used for dose calculation. Because of the absence of data for the whole region, the equal consumption of fish among the five modeled types was assumed.

The effective annual dose due to drinking seawater after desalination $E_{drink,k}$ (Sv a^{-1}) for a given radionuclide is described as follows:

$$E_{drink,k} = C_{dep} DC_k C_{w,k} CR_w \tag{5}$$

where $C_{w,k}$ is the concentration of k-th radionuclide activity in the water in the box where the desalinated plant is located, CR_w is the annual human consumption rate (m^3 a^{-1}) for desalinated water, and C_{dep} is the coefficient of depuration that corresponds to the part of radionuclides that remained in the water after desalination. According to [46,47], the desalination plant can remove the radioactive elements with from 90 to 99% efficiency. To be on the conservative side, for dose evaluations, the efficiency of the desalination plant was taken at 90% for removing radionuclides. Therefore, the value C_{dep} = 0.1 was used. The average recommended value of daily human consumption of water [48] is 3.2 L d^{-1}, which corresponds to CR_w = 1.168 m^3 a^{-1}. This value was used in the calculations of dose using Equation (5).

The changes over the time of annual dose due to the consumption of the marine products in the several boxes along the Gulf to the time after the deposition of radionuclides released from the Bushehr and Barakah NPPs are given in Figure 14. As seen in the figure, the annual dose can exceed the limited value for population 1 mSv or be quite close to it in the first year after accidents of such magnitude.

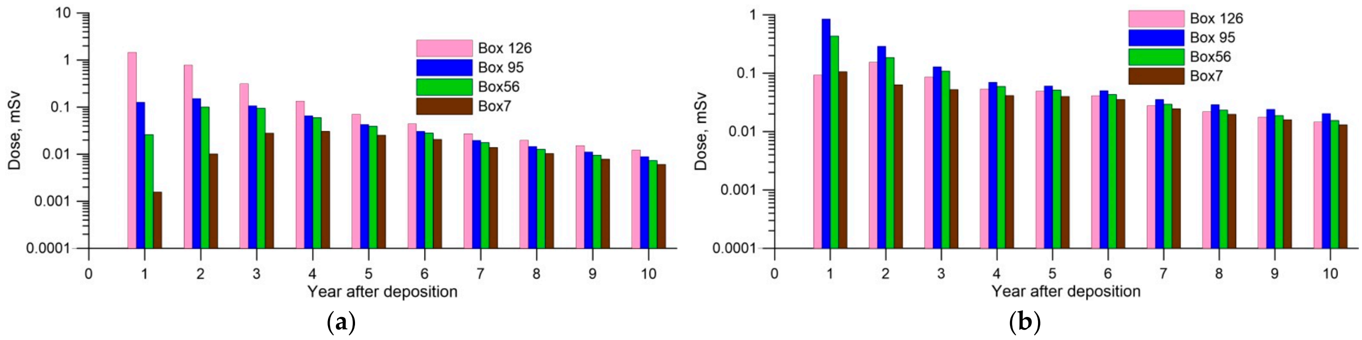

Figure 14. (**a**) Annual dose change in the several boxes over time after the deposition of radionuclides released from the Busher NPP; (**b**) annual dose change in the several boxes over time after the deposition of radionuclides released from the Barakah NPP.

The changes over time of the annual dose due to the drinking water consumption from four desalination plants (Figure 2a) in the Gulf after the deposition of radionuclides released from the Bushehr and Barakah NPPs are shown in Figure 15. As seen in the figure, these annual dose rates were at order less that the annual dose rates due to the consumption of the marine products. They did not exceed 0.2 mSv in the first year for either hypothetical accidents. The maximal annual dose after the hypothetical accident in the Bushehr NPP was in the location of the Doha desalination plant, whereas after the accident in the Barakah NPP, the maximal dose in the first year was in the Al Jubail and Ras Laffan desalination plants.

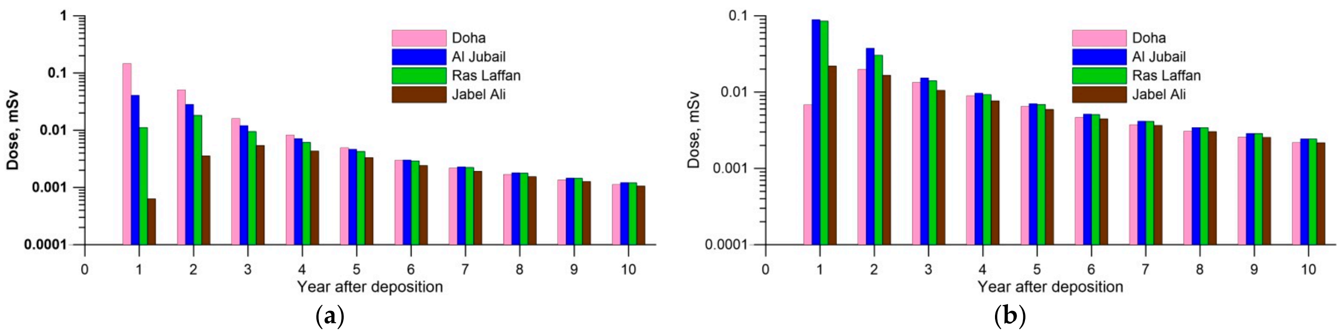

Figure 15. (**a**) Annual dose change in the vicinity of the desalination plants over time after the deposition of radionuclides released from the Bushehr NPP; (**b**) annual dose change in the vicinity of the desalination plants over time after the deposition of radionuclides released from the Barakah NPP.

The contribution of elements to the first-year accident dose depends on the type of reactor. Table 3 shows the contribution of elements to the dose as a result of hypothetical accidents at the Bushehr and Barakah NPPs. As can be seen, for reactor VVER-1000, the contribution of ^{134}Cs and ^{137}Cs to the dose dominates, being about 90%, whereas, for reactor APR-1400, the contribution of ^{106}Ru in the dose is 72% (see discussion in Section 4). This is also manifested in the differences between the contributions of different marine organisms to the dose, as shown in Table 4. As a result of a hypothetical accident at the Bushehr NPP, pelagic fish and crustaceans are the main contributors to the first-year dose. The benthic organisms play a more important role in subsequent years. At the same time, as a result of a hypothetical accident at the Barakah station, crustaceans make the largest contribution to the dose. This is due to the fact that the ^{106}Ru BAF of fish is relatively small (BAF = 2 L kg^{-1}) compared to the BAF of crustaceans (BAF = 100 L kg^{-1}).

Table 3. The contribution of elements to the dose as a result of hypothetical accidents at the Bushehr and Barakah NPPs.

Radionuclide	Bushehr NPP		Barakah NPP	
	Dose, mSv	%	Dose, mSv	%
^{134}Cs	1.18	79.84	0.16	19.14
^{137}Cs	0.17	11.57	0.07	7.85
^{106}Ru	0.10	6.83	0.61	72.11
^{90}Sr	0.03	1.76	0.0075	0.90

Table 4. The contribution of marine organisms to the dose as a result of hypothetical accidents at the Bushehr and Barakah NPPs.

Organism	Bushehr NPP		Barakah NPP	
	Dose, mSv	%	Dose, mSv	%
Non-piscivorous fish	0.47	31.89	0.09	10.77
Piscivorous fish	0.35	23.89	0.06	6.94
Demersal fish	0.022	1.50	0.0039	0.47
Bottom predatory fish	0.11	7.57	0.034	2.33
Coastal predators	0.19	12.72	0.0196	3.87
Crustaceans	0.33	22.43	0.64	75.62

Doses caused by sea spray inhalation, swimming, boating, and shoreline activity were calculated based on the methodology described in reference [27]. Reference values for occupancy time were selected from reference [49] for each type of activity. It was found that the sum of the doses from these four pathways of human exposure is an order of magnitude less than the dose from the drinking of desalinated water, which in turn, is an order of magnitude less than the dose from seafood consumption.

4. Discussion and Summary

In this study for the first time, the long-term consequences of radionuclide contamination of the Arabian Gulf as a result of hypothetical nuclear accidents at the Bushehr and Barakah NPPs were considered. This was achieved by performing simulations with a linked chain of models that account for atmospheric transport and deposition, the transfer of radioactivity in the marine food chain, and the formation of human doses through the marine pathways. Accordingly, the model chain included the atmospheric dispersion model RIMPUFF, the marine compartment model POSEIDON-R, complemented by a dynamical model for the transfer of radionuclides in the food chains, and the dose model. The representation of the radionuclide uptake by marine fish was improved by using an approach based on a tissue-weighted whole-body elimination rate. This approach allowed for a more accurate description of the assimilation of radionuclides, which are mostly accumulated in different tissues of fish. Unlike other studies, the meteorological scenarios were selected from real historical weather data for 5 years to provide a conservative estimation of the deposition of radionuclides in the Arabian Gulf.

With a limited water exchange through the Strait of Hormuz in the relatively shallow Gulf, the consequences of the release of radioactivity as a result of the accident at an NPP can be long-term, since a significant part of the released radionuclides will be deposited in the bottom, which serves as a source of water contamination for a long period of time. Long-term radionuclide contamination of the Gulf as a result of hypothetical accidents at two operating NPPs, Bushehr and Barakah, were simulated using a chain of models including the atmospheric dispersion model RIMPUFF, the compartment model POSEIDON-R, and the dose model. The source terms for the hypothetical releases of the selected radionuclides (^{134}Cs, ^{137}Cs, ^{106}Ru, and ^{90}Sr) in the atmosphere were defined based on respective reactor inventories available in the literature for VVER-1000 reactor. Hence the obtained results for Barakah NPP that operates APR-1400 reactor are more uncertain than the results for Bushehr NPP. Because emissions of ^{106}Ru, were less studied as compared to other radionuclides, the obtained concentrations of this radionuclide in fish and respective doses could be considerably overestimated and highly conservative. Conservative meteorological scenarios for the calculation of the initial depositions of radionuclides were selected based on the processing of historical weather data for 5 years and the simulation of the multiple series of dispersion scenarios. As shown in this study, in the selected conservative meteorological scenarios, more than 90% of the radioactivity is deposited on the surface of the Gulf. Because the Gulf is shallow, a significant part of the reactive radionuclides (^{134}Cs, ^{137}Cs, ^{106}Ru) remain in the bottom sediments and continue to contaminate water and benthic organisms for a long period of time. According to our study, even 50 years after the hypothetical accidents, the concentration of ^{137}Cs in the bottom sediments will be about 30 times higher than that in the current background concentration, which is 1–3 Bq kg^{-1} [42]. The corresponding concentration of ^{137}Cs in the water will be 5–8 Bq m^{-3}, which is also higher than the current background concentration of 1.25–1.38 Bq m^{-3} [42]. This means that many years after the accident, a large difference between pelagic and benthic organisms will remain. For example, the calculated concentration of ^{137}Cs in fish 50 years after the accident varies between 0.5 Bq kg^{-1} WW for non-predatory fish and 6.7 Bq kg^{-1} WW for coastal predators, whereas the current background concentration in fish is less than 0.034 Bq kg^{-1} WW [42].

In general, two main factors define the contamination of the Arabian Gulf as a result of a possible nuclear accident: (i) a source term that characterizes the rank of the accident and the amount of radioactive materials entering the environment; (ii) atmospheric conditions, which are responsible for the direction of the atmospheric transfer of the radioactive cloud and the intensity of deposition on the Gulf. When radionuclides fall into the Gulf, they will remain there for a long period of time, gradually contaminating the bottom sediments and marine organisms. The results of modeling show that approximately 8 years after the accident, regardless of the initial contamination, the concentration of radionuclides becomes uniform in the water. However, the bottom sediments retain the initial plume, slowly transported by currents, for a very long period of time. Due to differences in the uptake-elimination rates, initially, pelagic non-predatory fish will be the most contaminated fish species in the Gulf. Later, other types of fish could have the highest concentrations, but it will be less than the initial maximum in pelagic non-predatory fish. After many years, the demersal fish become the most contaminated species; however, at that time, all concentrations will decrease by several orders of magnitude.

Since the Arabian Gulf is the source of food (fishing industry) and water (desalination capabilities) for many people, safety becomes an important issue. For the first time, we estimated doses for the Gulf area according to the consumption of marine products, drinking water from desalination plants, sea spray inhalation, swimming, boating, and shoreline activity after accidents at two operating NPPs. According to the obtained results, the annual dose due to the consumption of marine products can exceed the maximum allowable value of 1 mSv, whereas the annual dose due to the drinking of water from desalination plants was an order less, due to the high efficiency of the desalination process for removing radionuclides (90%). In turn, doses caused by sea spray inhalation, swimming, boating, and shoreline activity were an order of magnitude less than the dose from drinking desalinated water. Analysis of the contribution of different marine organisms to the dose allows for the correct selection of countermeasures and the timing of their applications. For example, a ban on fishing in some parts of the Gulf or recommendations to exclude some species from the human diet can be introduced.

In summary, our study demonstrated the importance of marine pathways for long-term human exposure to radiation following a hypothetical nuclear accident in the area of the Arabian Gulf. The most important process in the long-term evolution of the contamination of the Gulf by reactive radionuclides is the interaction of bottom sediments with the water column. The model chain used for calculations, consisting of the atmospheric dispersion model, the compartment marine model, and the dose model, was customized for the area of the Gulf. The long-term prediction capabilities of the marine compartment model were demonstrated by the validation of the model predictions with the monitoring data after the Chernobyl and Fukushima Daiichi accidents, and due to the routine releases from the Sellafield and La Hague reprocessing plants. Gradual changes in the mean annual circulation and volume of the compartments as a result of climate change can be taken into account in future models. The model chain could be further used for long-term predictions of the radiological risks caused by potential nuclear accidents in the Gulf. The revised assessments may be performed both for refined release scenarios for the Barakah and Bushehr NPPs and for the new NPPs that are planned to be built in this area.

Supplementary Materials: The following supporting information can be downloaded at: https://www.mdpi.com/article/10.3390/jmse11020331/s1. Table S1. List of meteorological stations used for verification of calculated precipitation intensities. Table S2. Total deposition on the surface of the Arabian Gulf calculated by RIMPUFF and DIPCOT atmospheric dispersion models for scenarios of accidents at Bushehr and Barakah NPP, described in paper; the relative difference between both estimates $R = 100\% \cdot (Q_{RIMPUFF} - Q_{DIPCOT})/Q_{RIMPUFF}$ is presented in the last column. Figure S1. Precipitation intensities calculated by WRF (line) for the period 24–29 December 2015 compared with respective measurements (circles) extracted from Wolfram database https://reference.wolfram.com/language/ref/WeatherData.html, accessed on 12 December 2022. Figure S2. Precipitation intensities calculated by WRF (line) for the period 21–26 November 2017 compared with respective measurements (circles) extracted from Wolfram database https://reference.wolfram.com/language/ref/WeatherData.html, accessed on 12 December 2022. Figure S3. Maps of total (dry+wet) deposition density of (a) ^{134}Cs, (b) ^{106}Ru, (c) ^{90}Sr simulated by JRODOS system for the hypothetical accident scenario at Bushehr NPP started on 24 December 2015, 08:00 h UTC; deposition maps are dated 96 h after the start of the accident scenario. Figure S4. Maps of total (dry + wet) deposition density of (a) ^{134}Cs, (b) ^{106}Ru, (c) ^{90}Sr simulated by JRODOS system for the hypothetical accident scenario at Barakah NPP started on 21 November 2017, 15:43 h UTC; deposition maps are dated 96 h after the start of the accident scenario. Figure S5. Distribution of the ^{134}Cs concentration in water (Bq m^{-3}) at the Arabian Gulf surface after deposition for the hypothetical accident scenario at Bushehr NPP. Figure S6. Distribution of the ^{106}Ru concentration in water (Bq m^{-3}) at the Arabian Gulf surface after deposition for the hypothetical accident scenario at Bushehr NPP. Figure S7. Distribution of the ^{90}Sr concentration in water (Bq m^{-3}) at the Arabian Gulf surface after deposition for the hypothetical accident scenario at Bushehr NPP. Figure S8. Distribution of the ^{134}Cs concentration in the upper layer of sediment (Bq kg^{-1}) at the Arabian Gulf surface after deposition for the hypothetical accident scenario at Bushehr NPP. Figure S9. Distribution of the ^{106}Ru concentration in the upper layer of sediment (Bq kg^{-1}) at the Arabian Gulf surface after deposition for the hypothetical accident scenario at Bushehr NPP. Figure S10. Distribution of the ^{90}Sr concentration in the upper layer of sediment (Bq kg^{-1}) at the Arabian Gulf surface after deposition for the hypothetical accident scenario at Bushehr NPP. Figure S11. Distribution of the ^{134}Cs concentration in water (Bq m^{-3}) at the Arabian Gulf surface after deposition for the hypothetical accident scenario at Barakah NPP. Figure S12. Distribution of the ^{106}Ru concentration in water (Bq m^{-3}) at the Arabian Gulf surface after deposition for the hypothetical accident scenario at Barakah NPP. Figure S13. Distribution of the ^{90}Sr concentration in water (Bq m^{-3}) at the Arabian Gulf surface after deposition for the hypothetical accident scenario at Barakah NPP. Figure S14. Distribution of the ^{134}Cs concentration in the upper layer of sediment (Bq kg^{-1}) at the Arabian Gulf surface after deposition for the hypothetical accident scenario at Barakah NPP. Figure S15. Distribution of the ^{106}Ru concentration in the upper layer of sediment (Bq kg^{-1}) at the Arabian Gulf surface after deposition for the hypothetical accident scenario at Barakah NPP. Figure S16. Distribution of the ^{90}Sr concentration in the upper layer of sediment (Bq kg^{-1}) at the Arabian Gulf surface after deposition for the hypothetical accident scenario at Barakah NPP.

Author Contributions: Conceptualization, V.M. and R.B.; methodology, V.M. and I.K.; software, O.K.; investigation, R.B. and O.K.; writing—original draft preparation, V.M. and R.B.; writing—review and editing, I.K. and I.B.; visualization, I.B and O.K. All authors have read and agreed to the published version of the manuscript.

Funding: This research received no external funding.

Institutional Review Board Statement: Not applicable.

Informed Consent Statement: Not applicable.

Data Availability Statement: Not applicable.

Acknowledgments: The authors are grateful to the three anonymous reviewers and academic editor for their valuable suggestions that helped to improve the manuscript.

Conflicts of Interest: The authors declare no conflict of interest. The funders had no role in the design of the study; in the collection, analyses, or interpretation of data; in the writing of the manuscript, or in the decision to publish the results.

References

1. Le Quesne, W.J.F.; Fernand, L.; Ali, T.S.; Andres, O.; Antonpoulou, M.; Burt, J.A.; Dougherty, W.W.; Edson, P.J.; El Kharraz, J.; Glavan, J.; et al. Is the development of desalination compatible with sustainable development of the Arabian Gulf? *Mar. Pollut. Bull.* **2021**, *173*, 112940. [CrossRef]
2. World Nuclear Association. Plans For New Reactors Worldwide. Available online: https://world-nuclear.org/information-library/current-and-future-generation/plans-for-new-reactors-worldwide.aspx (accessed on 18 January 2023).
3. Terada, H.; Katata, G.; Chino, M.; Nagai, H. Atmospheric discharge and dispersion of radionuclides during the Fukushima Daiichi Nuclear Power Plant accident. Part II: Verification of the source term and analysis of regional-scale atmospheric dispersion. *J. Environ. Radioact.* **2012**, *112*, 141–154. [CrossRef] [PubMed]
4. Dvorzhak, A.; Puras, C.; Montero, M.; Mora, J.C. Spanish experience on modeling of environmental radioactive contamination due to Fukushima Daiichi NPP accident using JRODOS. *Environ. Sci. Technol.* **2012**, *46*, 11887–11895. [CrossRef] [PubMed]
5. Evangeliou, N.; Balkanski, Y.; Cozic, A.; Møller, A.P. Simulations of the transport and deposition of ^{137}Cs over Europe after the Chernobyl Nuclear Power Plant accident: Influence of varying emission-altitude and model horizontal and vertical resolution. *Atmos. Chem. Phys.* **2013**, *13*, 7183–7198. [CrossRef]
6. Bezhenar, R.; Kovalets, I. Modeling of radioactive contamination of the Black Sea and its impact on humans due to hypothetical heavy accident at the Zaporizhzhia NPP. In *Mathematical Modeling and Simulation of Systems. MODS 2022. Lecture Notes in Networks and Systems*; Shkarlet, S., Morozov, A., Palagin, A., Vinnikov, D., Stoianov, N., Zhelezniak, M., Kazymyr, V., Eds.; Springer: Cham, Switzerland, 2023.
7. Periáñez, R.; Bezhenar, R.; Brovchenko, I.; Duffa, C.; Iosjpe, M.; Jung, K.T.; Kim, K.O.; Kobayashi, T.; Liptak, L.; Little, A.; et al. Marine radionuclide transport modelling: Recent developments, problems and challenges. *Environ. Model. Softw.* **2019**, *122*, 104523. [CrossRef]
8. Tsabaris, C.; Tsiaras, K.; Eleftheriou, G.; Triantafylou, G. ^{137}Cs ocean distribution and fate at East Mediterranean Sea in case of a nuclear accident in Akkuyu Nuclear Power Plant. *Prog. Nucl. Energy* **2021**, *139*, 103879. [CrossRef]
9. Periáñez, R. APERTRACK: A particle-tracking model to simulate radionuclide transport in the Arabian/Persian Gulf. *Prog. Nucl. Energy* **2021**, *142*, 103998. [CrossRef]
10. Periáñez, R.; Cortés, C. A Numerical model to simulate the transport of radionuclides in the Western Mediterranean after a nuclear accident. *J. Mar. Sci. Eng.* **2023**, *11*, 169. [CrossRef]
11. Brovchenko, I.; Kim, K.O.; Maderich, V.; Jung, K.T.; Bezhenar, R.; Ryu, J.H.; Min, J.E. Sediment and radioactivity transport in the Bohai, Yellow, and East China Seas: A modeling study. *J. Mar. Sci. Eng.* **2022**, *10*, 596. [CrossRef]
12. Li, Z.; Zhou, T.; Zhang, B.; Si, G.; Ali, M. Research on radionuclide migration in coastal waters under nuclear leakage accident. *Prog. Nucl. Energy* **2020**, *118*, 103114. [CrossRef]
13. Yu, P.K.N. Trans-oceanic transport of ^{137}Cs from the Fukushima nuclear accident and impact of hypothetical Fukushima-like events of future nuclear plants in Southern China. *Sci. Total Environ.* **2015**, *508*, 128–135. [CrossRef]
14. IAEA. *Generic Models for Use in Assessing the Impact of Discharges of Radioactive Substances to the Environment*; Safety Reports Series 19; International Atomic Energy: Vienna, Austria, 2001.
15. Kamyab, A.; Azad, M.T.; Sadeghi, M.; Akhound, A. Dispersion simulation of cesium-137 released from a hypothetical accident at the Bushehr nuclear power plant in Persian Gulf. *Int. J. Coast. Offshore Environ. Eng.* **2018**, *2*, 13–17. [CrossRef]
16. Hassanvand, M.; Mirnejad, Z. Hydrodynamic model of radionuclide dispersion during normal operation and accident of Bushehr nuclear power plant. *Prog. Nucl. Energy* **2019**, *116*, 115–123. [CrossRef]
17. HYCOM. Available online: https://www.hycom.org/dataserver (accessed on 2 December 2022).
18. Mikkelsen, T.; Thykier-Nielsen, S.; Hoe, S. Chapter 2.16 Medium-range puff growth. In *Air Pollution Modeling and Its Application*; Borrego, C., Renner, E., Eds.; XVIII, Developments in Environmental Science; Elsevier: Amsterdam, The Netherlands, 2007; Volume 6, pp. 243–252. [CrossRef]
19. Bezhenar, R.; Heling, R.; Ievdin, I.; Iosjpe, M.; Maderich, V.; Willemsen, S.; de With, G.; Dvorzhak, A. Integration of marine food chain model POSEIDON in JRODOS and testing versus Fukushima data. *Radioprotection* **2016**, *51*, S137–S139. [CrossRef]
20. JRODOS. Available online: https://resy5.iket.kit.edu/JRODOS (accessed on 30 November 2022).
21. Zhuang, S.; Fang, S.; Dong, X. Local-Scale Atmospheric Dispersion Modelling of Radionuclides Following the Fukushima Daiichi Nuclear Accident Using SWIFT-RIMPUFF. In Proceedings of the 2022 29th International Conference on Nuclear Engineering, Virtual Online, 8–12 August 2022; Volume 15. V015T16A031. [CrossRef]

22. Andronopoulos, S.; Davakis, E.; Bartzis, J.G.; Kovalets, I. RODOS meteorological pre-processor and atmospheric dispersion model DIPCOT: A model suite for radionuclides dispersion in complex terrain. *Radioprotection* **2010**, *45*, S77–S84. [CrossRef]
23. Jafarikia, S.; Feghhi, S.A.H. Study of in-containment source term behavior for VVER-1000 under LOCA conditions using the IRBURN code system. *Ann. Nucl. Energy* **2018**, *112*, 17–29. [CrossRef]
24. Energoatom. *Additional Targeted Re-Evaluation of Safety of the Reactors of Zaporizhzhia NPP with Taking into Account Fukushima Lessons*; National Atomic Energy Generating Company 'Energoatom': Kyiv, Ukraine, 2012.
25. KEPCO. APR Design Control Document TIER 2. Chapter 15 Transient and Accident Analyses, Revision 3, Korea Electric Power Corporation & Korea Hydro & Nuclear Power Co., Ltd. 2018. Available online: https://www.nrc.gov/docs/ML1500/ML15006A042.pdf (accessed on 10 November 2022).
26. Lepicard, S.; Heling, R.; Maderich, V. POSEIDON/RODOS model for radiological assessment of marine environment after accidental releases: Application to coastal areas of the Baltic, Black and North seas. *J. Environ. Radioact.* **2004**, *72*, 153–161. [CrossRef] [PubMed]
27. Maderich, V.; Bezhenar, R.; Tateda, Y.; Aoyama, M.; Tsumune, D.; Jung, K.T.; de With, G. The POSEIDON-R compartment model for the prediction of transport and fate of radionuclides in the marine environment. *MethodsX* **2018**, *5*, 1251–1266. [CrossRef]
28. Bezhenar, R.; Jung, K.T.; Maderich, V.; de With, G.; Willemsen, S.; Qiao, F. Transfer of radiocaesium from contaminated bottom sediments to marine organisms through benthic food chain in post-Fukushima and post-Chernobyl periods. *Biogeoscience* **2016**, *13*, 3021–3034. [CrossRef]
29. IAEA (International Atomic Energy Agency). *Sediment Distribution Coefficients and Concentration Factors for Biota in the Marine Environment*; Technical Report Series No 422; IAEA: Vienna, Austria, 2004; 95p.
30. Bezhenar, R.; Kim, K.O.; Maderich, V.; de With, G.; Jung, K.T. Multi-compartment kinetic-allometric (MCKA) model of radionuclide bioaccumulation in marine fish. *Biogeosciences* **2021**, *18*, 2591–2607. [CrossRef]
31. Yankovich, T.; Beresford, N.; Wood, M.; Aono, T.; Anderson, P.; Barnett, C.L.; Bennett, P.; Brown, J.E.; Fesenko, S.; Fesenko, J.; et al. Wholebody to tissue-specific concentration ratios for use in biota dose assessments for animals. *Radiat. Environ. Biophys.* **2010**, *49*, 549–565. [CrossRef]
32. Pouil, S.; Bustamante, P.; Warnau, M.; Metian, M. Overview of trace element trophic transfer in fish through the concept of assimilation efficiency. *Mar. Ecol. Prog. Ser.* **2018**, *588*, 243–254. [CrossRef]
33. Periañez, R.; Bezhenar, R.; Iosjpe, M.; Maderich, V.; Nies, H.; Osvath, I.; Outola, I.; de With, G. A comparison of marine radionuclide dispersion models for the Baltic Sea in the frame of IAEA MODARIA program. *J. Environ. Radioact.* **2015**, *139*, 66–77. [CrossRef]
34. CMEMS, Copernicus Marine Environment Monitoring Service. Available online: http://marine.copernicus.eu (accessed on 11 November 2022).
35. Alosairi, Y.; Imberger, J.; Falconer, R.A. Mixing and flushing in the Persian Gulf (Arabian Gulf). *J. Geophys. Res.* **2010**, *116*, C03029. [CrossRef]
36. Al-Ghadban, A.N. Assessment of suspended sediment in Kuwait bay using Landsat and spot images. *Kuwait J. Sci. Eng.* **2004**, *31*, 155–172.
37. Al-Ghadban, A.N.; Abdali, F.; Massoud, M.S. Sedimentation rate and bioturbation in the Arabian Gulf. *Environ. Int.* **1998**, *24*, 23–31. [CrossRef]
38. Skamarock, W.C.; Klemp, J.B.; Dudhia, J.; Gill, D.O.; Barker, D.; Duda, M.G.; Huang, X.Y.; Wang, W.; Powers, J.G. *A Description of the Advanced Research WRF Version 3*; (No. NCAR/TN-475+STR); University Corporation for Atmospheric Research: Boulder, CO, USA, 2008. [CrossRef]
39. GFS. NCEP GDAS/FNL 0.25 Degree Global Tropospheric Analyses and Forecast Grids. Research Data Archive at the National Center for Atmospheric Research, Computational and Information Systems Laboratory. National Centers for Environmental Prediction/National Weather Service/NOAA/U.S. Department of Commerce. 2015. Available online: https://rda.ucar.edu/datasets/ds083.3/ (accessed on 2 December 2022).
40. Wolfram Research, WeatherData, Wolfram Language Function. 2008. Available online: https://reference.wolfram.com/language/ref/WeatherData.html (accessed on 2 December 2022). (updated 2014).
41. Mahmoud, M.T.; Al-Zahrani, M.A.; Sharif, H.O. Assessment of global precipitation measurement satellite products over Saudi Arabia. *J. Hydrol.* **2018**, *559*, 1–12. [CrossRef]
42. Uddin, S.; Fowler, S.; Behbehani, M.; Al-Ghadban, A.; Swarzenski, P.; Al-Awadhi, N. A review of radioactivity in the Gulf region. *Mar. Pollut. Bull.* **2020**, *159*, 111481. [CrossRef]
43. ICRP (International Commission on Radiological Protection). Corrigenda to ICRP Publication 119: Compendium of Dose Coefficients based on ICRP Publication 60. *Ann. ICRP* **2013**, *42*, 1–130. [CrossRef]
44. ICRP (International Commission on Radiological Protection). *Compendium of Dose Coefficients based on ICRP Publication 60*; Elsevier: Amsterdam, The Netherlands, 2012; Volume 41.
45. FAO (Food and Agricultural Organization). GLOBEFISH Market Profile. Information and Analysis on Markets and Trade of Fisheries and Aquaculture Products. Available online: https://www.fao.org/in-action/globefish/countries/en/ (accessed on 12 December 2022).
46. IAEA (International Atomic Energy Agency). *Safety Aspects of Nuclear Plants Coupled with Seawater Desalination Units*; IAEA-Tecdoc-1235; IAEA: Vienna, Austria, 2001.

47. Calvert Cliffs Nuclear. Power Plant Unit 3. Combined License Application. Part 3: Environmental Report. Rev.8, UniStar Nuclear Services, LLC. 2012. Available online: https://www.nrc.gov/docs/ML1213/ML12137A082.pdf (accessed on 12 December 2022).
48. Perry, C.; Gans, K. Here's How Much Water You Should Drink a Day, According to Experts. Forbes Health. 2022. Available online: https://www.forbes.com/health/body/how-much-water-you-should-drink-per-day (accessed on 12 December 2022).
49. Nielsen, S.; Bengtson, P.; Bojanowsky, R.; Hagel, P.; Herrmann, J.; Ilus, E.; Jakobson, E.; Motiejunas, S.; Panteleev, Y.; Skujina, A.; et al. The radiological exposure of man from radioactivity in the Baltic Sea. *Sci. Total Environ.* **1999**, *237*, 133–141. [CrossRef] [PubMed]